

Dynamics of two-electron photoemission from Cu(111)

M. Hattass,^{1,*} T. Jahnke,¹ S. Schössler,¹ A. Czasch,¹ M. Schöffler,¹ L. Ph. H. Schmidt,¹ B. Ulrich,¹ O. Jagutzki,¹ F. O. Schumann,² C. Winkler,² J. Kirschner,² R. Dörner,¹ and H. Schmidt-Böcking¹

¹*Institut für Kernphysik, Johann Wolfgang Goethe Universität, Max-von-Laue-Strasse 1, 60438 Frankfurt, Germany*

²*Max Planck-Institut für Mikrostrukturphysik, Weinberg 2, 06120 Halle/Saale, Germany*

(Received 27 February 2008; revised manuscript received 3 April 2008; published 30 April 2008)

By using a new imaging technique for pairs of electrons emitted in coincidence from a surface, we investigated the two-electron photoemission from a Cu(111) surface in the energy range from $\hbar\omega=40$ to 60 eV. The full solid angle coverage provides a comprehensive view into the details of the emission process and allows for a quantitative study of the exchange-correlation (XC) hole in the two-electron momentum final state. Evaluating the data in a center-of-mass frame the XC hole yields a value of ~ 0.76 a.u. as smallest distance in momentum space. Additionally, we can demonstrate a significant dependency of the emission dynamics on the light polarization.

DOI: [10.1103/PhysRevB.77.165432](https://doi.org/10.1103/PhysRevB.77.165432)

PACS number(s): 79.60.Bm, 73.20.-r

I. INTRODUCTION

The process of double ionization of atoms and molecules is one of the toughest touchstones for the theory of dynamic atomic and molecular systems. As the ejection of two electrons by a single photon is prohibited in a single particle picture, the investigation of this effect is a sensitive probe for electronic correlation in the bound state.^{1–8} While considerable progress has been made in the understanding of the double ionization process in gaseous targets (see Refs. 9–11 for a review), the complementary process at surfaces has not been studied in comparable depth so far. However, for solid state physics double photoemission (DPE) is a promising tool to gain access to important parameters of a solid that rely on the mutual electron interaction. Electrons in a solid interact via their mutual Coulomb interaction as well as Pauli's exclusion principle. This leads to the formation of the exchange correlation (XC) hole, i.e., a reduced probability to find a second electron in the vicinity of another one.¹⁶ The extension of the hole is of fundamental interest for solid state physics as it is a main conclusion of the local density approximation^{12,13} that is widely applied in the description of many-electron systems.

It has been shown theoretically that the XC hole can be imaged in the two-electron momentum final state of an DPE experiment.^{14,15} The development on the experimental side to detect two correlated electrons emitted by a single photon from a surface has advanced over the past years.^{17,18} Recently, the observation of the XC-correlation hole in the angular distribution of coincident electrons emitted from a LiF and Cu(111) surface has been reported.^{19,20}

In this paper, we present our results on the two-electron photoemission from a Cu(111) surface. The data have been obtained with a new experimental setup that is capable to image the full six-dimensional momentum space of the two emitted electrons. The fully differential data allow for a very comprehensive view of the emission dynamics and a new evaluation of the data in a center-of-mass frame.

II. EXPERIMENTAL SETUP

The described experiment has been conducted at beam line BW3 at HASYLAB/DESY in Hamburg. The experimen-

tal setup used in this study is sketched in Fig. 1. The photon beam laterally enters through an opening into the spectrometer and hits the sample surface. The ejected electrons are extracted from the sample surface by a weak electric field and accelerated along the Z axis toward a position and time sensitive detector. Additionally, a parallel homogeneous magnetic field is applied that forces the electron on a cyclotron motion in the XY plane. The combination of electric and magnetic fields allows for the detection of electrons in the energy range of interest over the full 2π hemisphere above the sample. The detector is equipped with a hexagonal delay line anode^{21,22} that is capable to detect several electrons position and time resolved with a very low dead time. By measuring time of flight and impact position the initial momenta can be reconstructed, yielding the complete six-dimensional two-electron momentum final state. The coincidence rate achieved with this setup is (at $\hbar\omega=40$ eV) about 20 counts/s with a contribution of random (two independent single photoemission events instead of a two-electron emission) of about 10%–15%. The single electron emission rate was tuned to about 3 kHz. All information for each event is

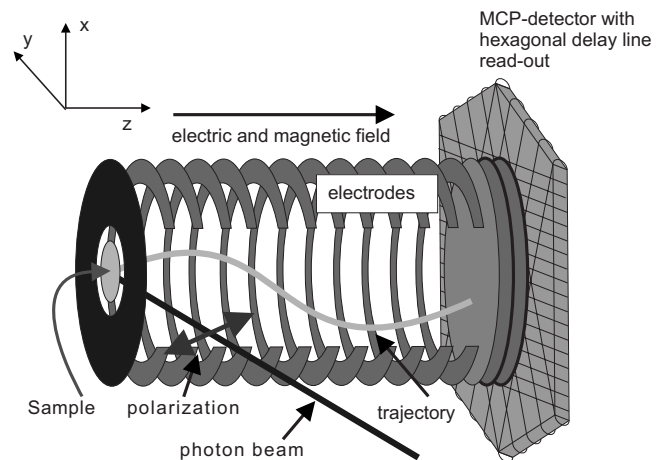


FIG. 1. Sketch of the experimental setup. The spectrometer axis lies along the z axis, and the sample in the XY plane. The light incidence angle is 45° to the surface normal with the polarization in the YZ plane.

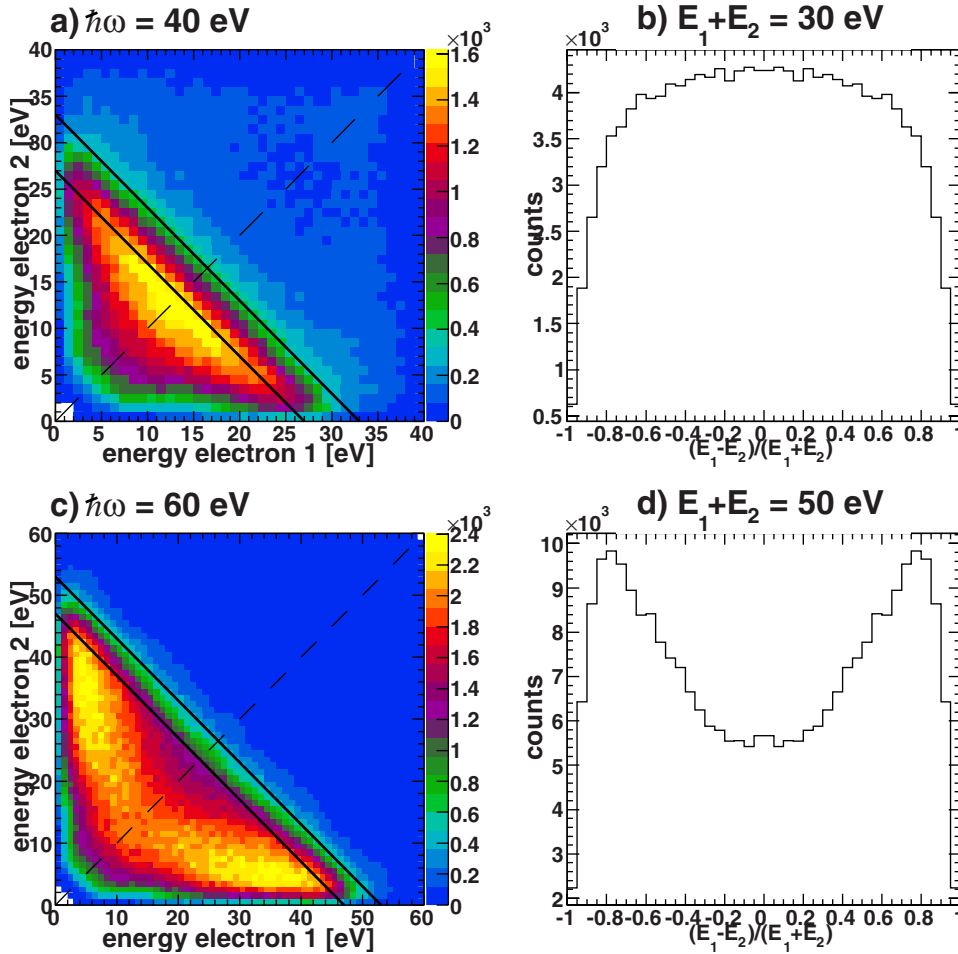


FIG. 2. (Color online) [(a) and (c)] Electron-electron energy spectrum for $\hbar\omega=40$ and 60 eV; the spectra have been mirrored at the diagonal broken line. [(b) and (d)] Electron energy sharing $[(E_1 - E_2)/(E_1 + E_2)]$ for sum energies in the area between the two solid lines.

stored in an event mode data acquisition system. This allows us to generate every projection and cut through the data later on in an off-line data analysis. A more detailed description of the apparatus can be found in Ref. 23

The light incidence angle is 45° to the surface normal, while the projection of the polarization on the surface lies along the Y axis, which coincides with the $[1\bar{1}0]$ direction of the Cu(111) surface. The crystal surface was prepared by multiple cycles of sputtering with 500 eV Ar^{1+} ions and subsequent annealing to 600°C , which were repeated every 8 h. The base pressure of the vacuum chamber was always kept below 5×10^{-10} mbar. The surface structure could be permanently monitored by using the data from (noncoincident) angle resolved single photoemission events, which have been collected parallel to the coincidence data.

III. RESULTS

Figure 2 shows the angle integrated two electron energy distribution for $\hbar\omega=40$ eV [Fig. 2(a)] and $\hbar\omega=60$ eV [Fig. 2(c)]. As the electrons are detected by a single detector, an unphysical preselection of events is done because the first detected electron will be in most cases the higher energetic one. To maintain the indistinguishability, the spectra are mirrored along the dashed diagonal line. In the following, this is done with all spectra, which would lead to a unequal treat-

ment of electron “1” and electron “2.” Both spectra show a clear cutoff at $E_1 + E_2 = 30$ and 50 eV, respectively. This upper limit is determined by the photon energy and the work function W_ϕ of the surface and is given by $E_1 + E_2 \leq \hbar\omega - 2W_\phi$ [$W_\phi = 4.94$ eV for Cu(111) (Ref. 24)]. This behavior was found in previous experiments at surfaces, $(\gamma, 2e)$ as well as $(e, 2e)$.¹⁸ The energy sharing $[(E_1 - E_2)/(E_1 + E_2)]$ of the electron pair near the cutoff rapidly changes in this energy regime, as shown in Figs. 2(b) and 2(d). While for 40 eV, there is a wide maximum for symmetric energy sharing near the threshold ($E_1 = E_2$), at 60 eV, the energy sharing is rather asymmetric (one fast, one slow electron). However, both spectra show a vanishing signal towards extreme unequal energy sharing. This finding is a consequence of the vanishing density of states (DOS) for very low energetic electrons near the vacuum level at surfaces.¹⁴ In contrast to the double ionization of a free atom, where the DOS for the emitted electrons scales as $1/k$, here (in terms of the three-step model of photoelectron emission from surfaces) the closing of the escape cone²⁴ leads to a strong suppression. We would like to point out that this feature is not explained by an experimental cutoff, as our setup is able to detect electrons at 0 eV kinetic energy at vacuum level due to the electrostatic extraction field.

To give an idea of the uncorrelated fraction—resulting from random coincidences of two electrons emitted by two different photons—in the spectra, no background substrac-

tion above the physical limit of $\hbar\omega - W_\phi$ has been applied to the images. For $\hbar\omega=40$ eV, the uncorrelated electron pairs can be found, e.g., in the region where both electrons carry about 30–35 eV total. These false coincidences clearly stem from two uncorrelated electrons emitted in single photoemission, mainly from the Cu 3*d* valence band. In turn, these false coincidences together with the simultaneously recorded single photoemission data allow for a good estimation of the contribution of uncorrelated electron pairs which lies around 15% for $\hbar\omega=40$ eV and about 10% for $\hbar\omega=60$ eV.

A. Correlation hole in the angular distribution

By using the angle resolving capability of our detector setup, we display now the data in a projection view to the sample surface. For that purpose, we use only the data of electrons with a fixed sum energy of the pair, i.e., electron pairs with a constant two-electron binding energy. Owing to the limited energy resolution of our setup the integration interval is set to $E1+E2=30\pm 3$ eV, while the photon energy is $\hbar\omega=40$ eV.

The first and third column of Fig. 3 display the full angular distribution of the electrons while the emission direction of the second is kept fixed as indicated by the full circle. The second and fourth columns are the projections of a $\pm 20^\circ$ slice of the full distribution on the *X* axis to the *Y* axis. Again, the emission direction of the fixed electron is indicated by the arrow. From top to bottom of Fig. 3, the energy sharing ratio of the pair is varied. We display the data where the fixed electron carries 10%, 30%, 50%, 70%, and 90% of the sum energy.

We focus first on the left two columns of Fig. 3 where the fixed electron is directed toward the center (emission along the surface normal). Following the change in energy sharing from top (fixed electron slow, displayed electron fast) to bottom (fixed electron fast, displayed electron slow), we can observe a decrease in intensity around the direction of the fixed electron. At equal energy sharing conditions, this gap is most pronounced and subsequently filled up again toward asymmetric energy sharing. The opening angle of the cone for equal energy sharing as measured to the maximum is about 50° . This finding is commonly regarded as the footprint of the XC hole, which is present in the two-electron photoemission process.¹⁴ The influence of the emission direction of the fixed electron on the second one becomes even more obvious when comparing Figs. 3(c)(I) and 3(c)(II) with Fig. 4(a), which shows the same energy sharing, while there is no preselection in angle for the first electron. Here, the central gap is filled up completely. Our data complement and confirm the recently published data from Schumann *et al.*²⁰ on the first observation of the XC hole on copper, which was obtained with an independent experimental setup (three detector arrangement), however, with a slightly different light incidence geometry (32° and $\hbar\omega=50$ eV) and energy sharing.

For a very unequal energy sharing the angular distribution nearly reflects the corresponding angular distribution without preselection in angle. This case is shown in Figs. 4(a) and 4(b) where the fast electron is plotted while the slow one is

fixed only in energy but not in angle. This is to be expected because here both electrons are well separated in momentum space. Hence, they will not influence each other's path significantly.

For an off-center emission of the fixed electron, we observe a similar trend. The corresponding data are shown in the two right columns of Fig. 3. Here, the emission direction of the fixed electron is set to an off-normal of 45° as indicated by the full circle [two-dimensional (2D) histograms] and the arrow (one-dimensional histograms), while again the angular distribution of the second one is plotted. At equal energy sharing, the depth of the gap around the first electron is most pronounced and is filled toward unequal sharing.

B. Correlation hole in the momentum distribution

The data clearly show a dependency of the relative emission angles of the two electrons and the existence of a depletion zone around the fixed electron, when both electrons are close in energy. Besides, the analysis of the experimental data in the angular space an alternative way is possible. As we will show below, the motion of a pair can be separated into the movement of the center of gravity and the relative motion. Such a notion in momentum space was put forward in a theoretical description.²⁵

The focus is now only on electron pairs which carry equal energies as for this combination we expect the strongest interaction, i.e., correlation. The data in momentum representation are shown in Fig. 5, where atomic units ($\hbar=e=m=1$) were used. Similar to the previously discussed angular distributions, the emission direction of the first electron is kept fixed as indicated by the circle (integration radius 0.2 a.u.) and the second one is shown. Figures 5(b) and 5(d) are projections of the data to the *Y* axis within a strip of ± 0.2 a.u. of the *x* axis. For Figs. 5(a) and 5(b), the first electron is emitted along the surface normal, while Fig. 5(c) and 5(d) show the distributions in case of an off-normal emission. In both cases, we observe a vanishing intensity of the signal when the two electrons are close in momentum space. The peaks in Fig. 5(b) are at ± 0.9 a.u., which is qualitatively in agreement with the calculation of the DPE intensity from a Cu(100) surface. The calculations showed that the fixed emission direction is surrounded by a reduced probability of finding the second electron. This was interpreted as to be a signature of the correlation hole. If we then take the peak positions in the distribution of Fig. 5(b) as measure of the size of correlation hole, then we note that those are somewhat further apart than the theory predicts. The calculated values are $\pm 0.7-0.8$ a.u. for a photon energy 42.4 eV and a kinetic energy of 16 eV of each electron.¹⁴ The energetics is therefore close to our experiment, which has a photon energy of 40 eV and the individual electrons have an energy of 15 eV. This deviation in size of the depletion zone in theory and experiment was observed also by Schumann *et al.* in line with our results. However, this deviation may be caused by the experimental boundary conditions: to acquire a significant amount of statistics the integration area for the first electron has to be chosen in an order comparable to the hole diameter. Consequently, this will smear out the rim of the

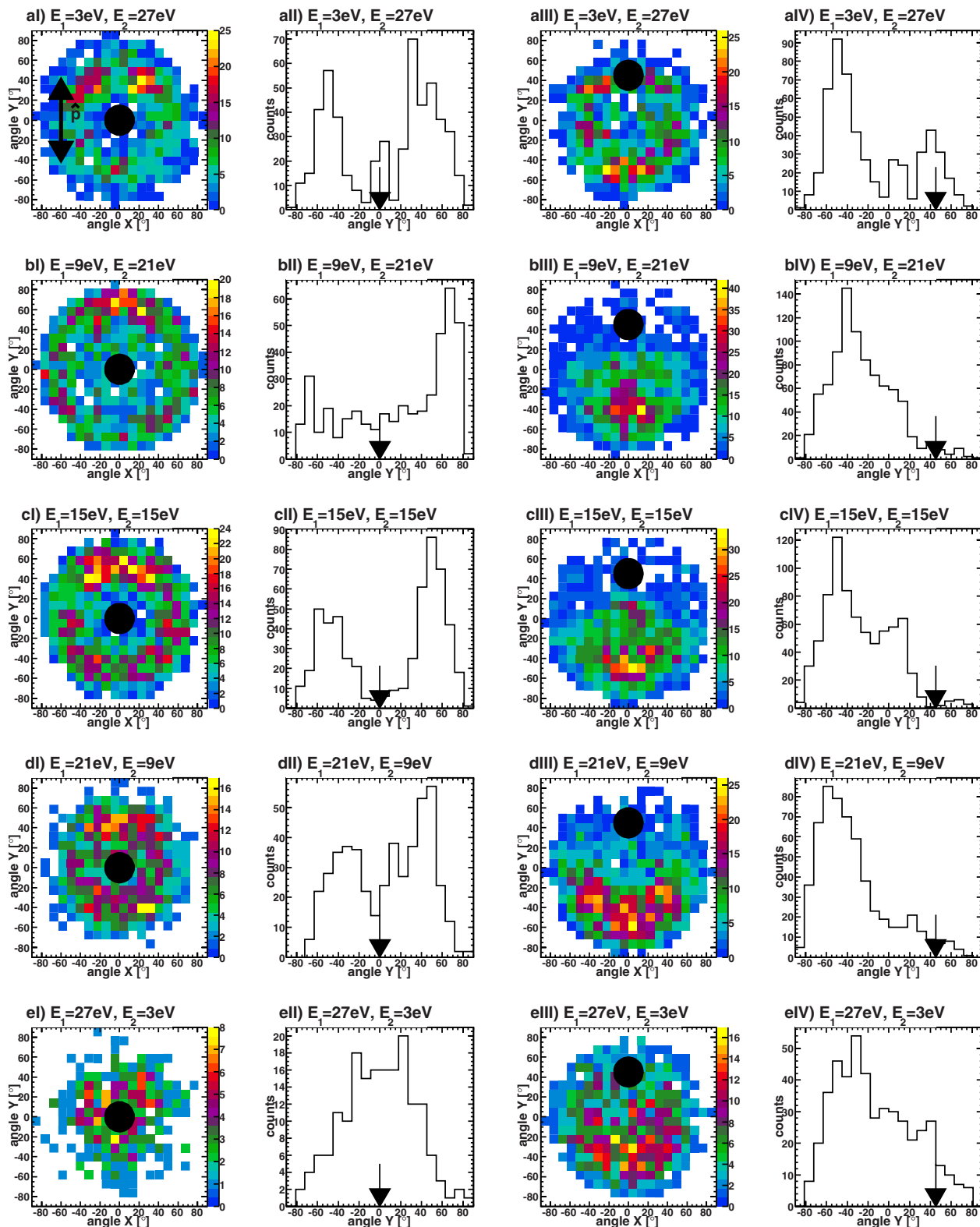


FIG. 3. (Color online) Angular distributions of one electron while the emission direction of the other on is kept fixed. The panels are read as follows: column (I) is a projection view onto the surface plane where the emission direction of the first electron is along the surface normal as indicated by the full circle. Column (II) contains the respective projections to the Y axis within the slice $\pm 20^\circ$ on the X axis. The emission direction of the fixed electron is indicated by the arrow. Column (III) is the same as column (I) but now with an emission of the first electron at an angle of 45° with the surface normal in the YZ plane. Column (IV) contains again the projections to the Y -axis. In rows (a)–(e), the energy sharing of the coincident pair is varied. The sum energy is constant $E_1 + E_2 = \hbar\omega - 2W_\phi \pm 3 \text{ eV}$; the photon energy is $\hbar\omega = 40 \text{ eV}$. The orientation of the light polarization is indicated by the arrow in panel (a) (I).

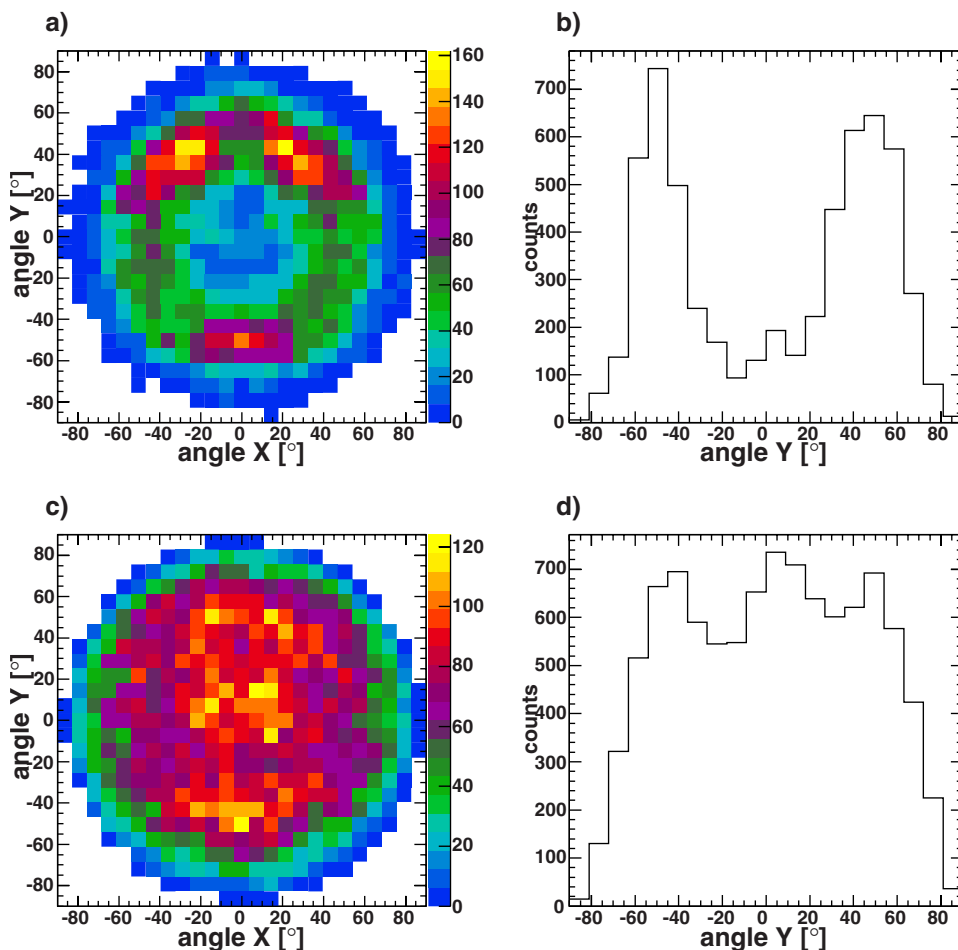


FIG. 4. (Color online) Angular distribution of the second photoelectron for a given energy sharing but without restriction angle for the first one. [(a) and (c)] Projection view onto the surface plane for 10% and 50% sharing and [(b) and (d)] respective projections of the slice $\pm 20^\circ$ on the X axis to the Y axis. $\hbar\omega$ is 40 eV and sum energies $E_1 + E_2 = \hbar\omega - 2W_\phi \pm 3$ eV, equal energy sharing. The orientation of the light polarization is given by the arrow.

hole and may complicate the interpretation of the results. To encounter this problem, we will suggest a different approach to quantitatively evaluate the correlation hole using the pair's center-of-mass motion.

Evaluation in the center-of-mass frame

It has been pointed out in the first theoretical treatment of the two-electron photoemission from solids by Berakdar²⁵ that the emitted electron pair constitutes a quasiparticle, which can be described by the motion of the center of mass and the relative motion. For the first part, the sum momentum K_+ is appropriate, whereas the relative motion is given by K_- . These quantities are computed from the individual momenta (k_1, k_2) of the electrons as follows:

$$K_+ = k_1 + k_2, \quad (1)$$

and the relative momentum K_-

$$K_- = \frac{1}{2}(k_1 - k_2). \quad (2)$$

Due to the crystalline surface, we know that the sum of the in-plane momenta of the electrons in the initial state and final state must be conserved modulo a reciprocal lattice vector. This is essentially a diffraction condition for the center-of-mass motion. One major result of the theoretical investigation is that the propensity rule $(k_1 + k_2) \cdot \hat{p}$, which is valid

for the double photo ionization of free atoms^{26,27} still holds approximately for localized and delocalized states in a solid, i.e., the DPE intensity will be reduced for electron pairs with sum momentum perpendicular to the polarization vector. An experimental test of this prediction and its validity is lacking. In Fig. 6, we plot the in-plane components (K_{+x} and K_{+y}) of the sum momenta in the surface for electron pairs with sum energies near the emission threshold ($E_1 + E_2 = \hbar\omega - 2W_\phi \pm 3$ eV). The left panels (a) and (c) contain the full distribution, while the right panels are projections to the Y axis of the interval $(-0.3, 0.3)$ a.u. between the two lines. The projection of the light polarization vector onto the surface plane is oriented as indicated by the arrow. We observe a preferential emission of electron pairs, whose sum momenta are shifted towards the positive Y axis. The maximum intensity is found at ~ 0.25 a.u. for $\hbar\omega = 40$ eV and ~ 1.1 a.u. for 60 eV, respectively. We do not observe any sharp diffraction peaks, which we associate with the large energy integration we need to perform. Since the 3d bands are relatively flat, we essentially sum over the whole Brillouin zone as far as the initial states are concerned. The broad maxima of the K_+ distributions may indicate a preferential contribution of certain initial states. The stronger intensity toward the positive Y axis, which can be explained by the geometry used in this experiment. Due to the non-normal incidence angle the polarization will induce two preferential emission directions: one toward the positive Y axis into the vacuum and a second

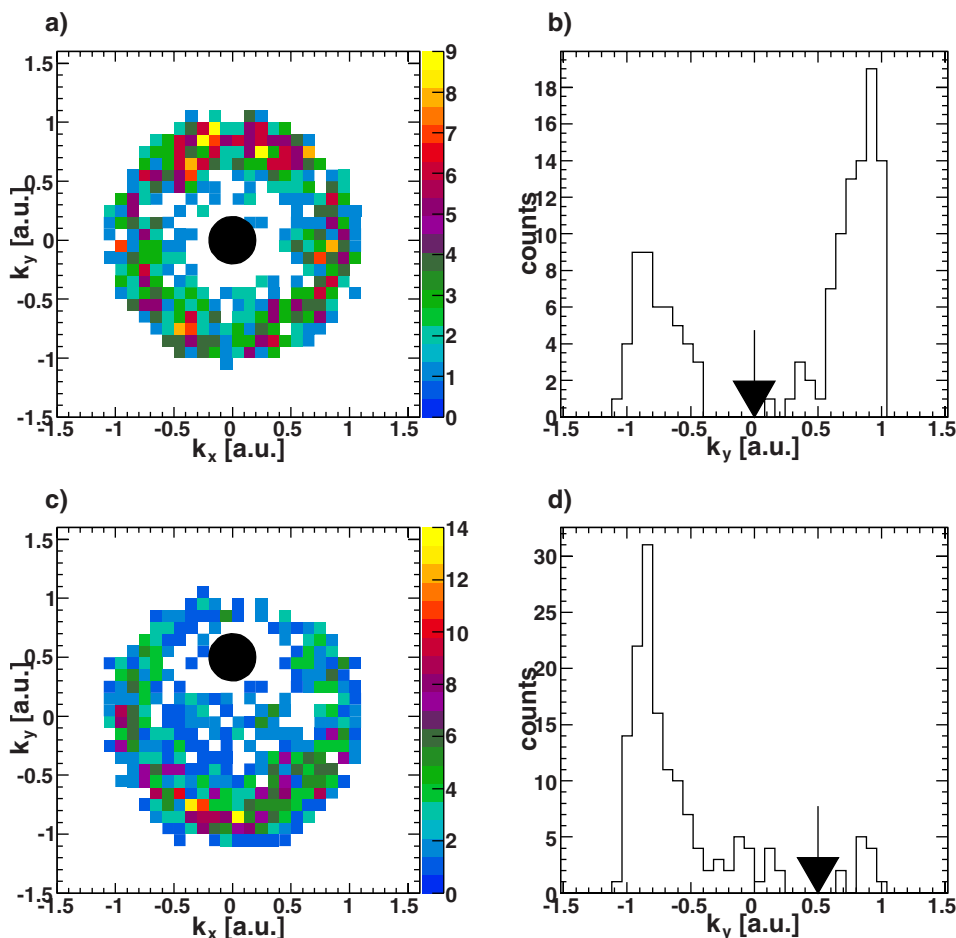


FIG. 5. (Color online) Momentum distributions parallel to the surface plane. The momentum of one electron is kept fixed, while the second one is plotted. The electron energies are $E_1=E_2=15$ eV; the photon energy is 40 eV. Panels (a) and (c) are the full momentum distributions in the XY plane. Panels (b) and (d) are the projections of the slice ± 0.2 a.u. on the X axis in (a) and (c) to the Y axis. The momentum of the fixed electron is indicated by the full circle in (a) and (c) and the arrow in (b) and (d).

one toward the negative Y axis into the solid. Consequently, electron pairs in the first case will more easily escape through the surface of solid than the ones in the latter case. To detect a pair which was emitted into the solid in the primary process, both electrons need an additional scattering to arrive at a momentum with values toward the positive Z axis. Obviously, the intensity for this process will be significantly lower as the effective path through the solid is much longer and electrons may be lost due to inelastic scattering.

Using the relative momentum K_- to evaluate the experimental data offers several practical advantages. First, the distance in momentum space is individually measured for each coincident electron event, i.e., one does not have to integrate over a certain region in momentum space which will—due to the finite size of the integration region—wash out the rim of the hole. Furthermore, the statistics can be significantly improved because it is possible to evaluate all emission combinations at once. This allows a much better measurement of the intensity contrast between the hole region and the surrounding varying intensity caused by the crystal face. An implicit assumption in this procedure is that the K_- distributions for different K_+ values can be directly compared.

To extract additional information on the different emission mechanism, we combine the scaling rule in the sum momenta with the evaluation in the relative momenta. As the primary DPE process will follow the scaling rule, which may help to separate different excitation pathways or to suppress coincident electrons from, e.g., multiple scattering. For that

purpose, we apply further restrictions on the distribution of relative momenta by at the same time requiring a specific orientation of the sum momentum. In the first case, the sum momentum is oriented parallel to the polarization vector, which should contain mostly events which have been created by the initial process.

In the second geometry, the sum momentum is perpendicular to the polarization vector, which should lead to a vanishing DPE intensity. This selection is achieved by only allowing events within the region $K_{+x} \in [-0.1, 0.1]$ or $K_{+y} \in [-0.1, 0.1]$ corresponding to the area between the horizontal and vertical dashed lines in Fig. 6(a). Figure 7 shows the data that have been filtered in the described way. Figures 7(a) and 7(b) correspond to $K_+ \parallel \hat{p}$, while Figs. 7(c) and 7(d) $K_+ \perp \hat{p}$. Figures 7(b) and 7(d) are the projections of Figs. 7(a) and 7(c) to the y axis for $K_{-x} \in [-0.3, 0.3]$. The photon energy is $\hbar\omega=40$ eV, $E_1=E_2=15$ eV. Both 2D-distribution spectra reveal a circular shape with a central decrease in intensity. In Fig. 7(a), the intensity reaches closer to the center and is more evenly distributed over the outer ring than for the distribution in Fig. 7(b), which shows a preferential emission along the y axis. This can be analyzed in more detail when changing to the projections along the y axis [Figs. 7(b) and 7(d)]. For the case $K_- \parallel \hat{p}$, a double peak structure appears. Evaluating the spectra with a two-peak Gaussian fit yields for the position of the maxima $\sim \pm 0.38$ and $\sim \pm 0.75$ a.u. For $K_- \perp \hat{p}$ [Fig. 7(d)], only one peak is left in the distribution with a slight shoulder towards smaller absolute values. A

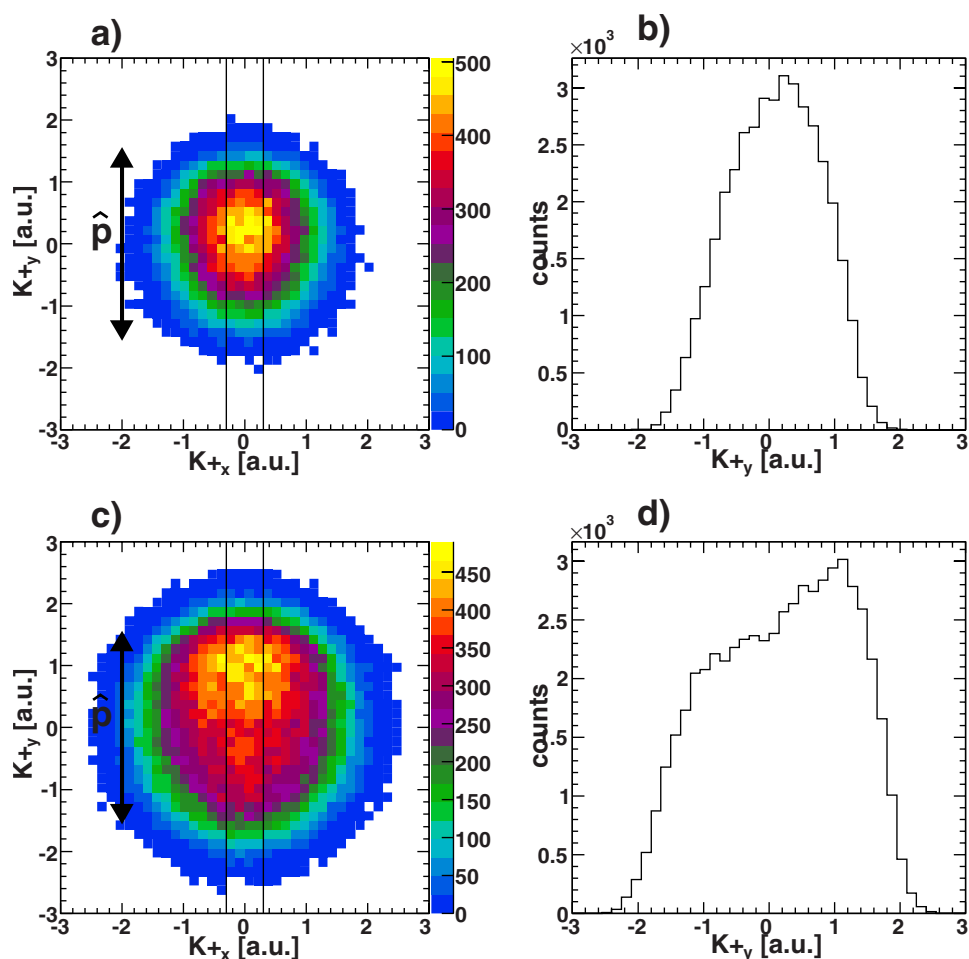


FIG. 6. (Color online) Center-of-mass momentum distribution parallel to the surface for $\hbar\omega=40$ and 60 eV. The sum energy is set to 30 and 50 eV, respectively. [(a) and (c)] Full 2D distributions and [(b) and (d)] projection of the area between the vertical lines to the y axis.

Gaussian fit results here in a maximum at $\sim \pm 0.79$ a.u..

An immediate interpretation could be that this is a signature of two different emission mechanisms. The first inner peaks in Fig. 7(b) can be regarded as created by the initial DPE process. These electron pairs can only appear for the case $K_+ \parallel \hat{p}$ and should disappear if $K_+ \perp \hat{p}$, which is clearly confirmed as shown in Fig. 7(d). In this case, one may determine the size of the opening of the XC hole, we find a value of ± 0.38 a.u. (i.e., a mean value of 0.76 a.u. when changing back to a laboratory frame), which agrees very well with the calculations by Fominykh *et al.*¹⁴ obtained for a Cu(100) surface. This suggests that the outer peaks in Fig. 7(b) at ± 0.75 a.u. are from processes, which do not dependent on the DPE scaling rule. One scenario, which comes to mind, is that these electron pairs are created in a $(e, 2e)$ collision, where the first electron “projectile” is a photoelectron from a single photoemission event. Due to the much higher probability to create a single photoelectron and the short mean free path of electrons in the given energy range, this process cannot *a priori* neglected. As a matter of fact emission of electron pairs from surfaces excited with a primary electron beam is a technique, which also allows us to access the XC hole. It was found that the fixed emission direction of one electron was surrounded by a reduced intensity of the other electron. The theoretical description of the $(e, 2e)$ process has also advanced over the recent years. A specific result relevant for our work deals with the pair emis-

sion from Cu(111) surface excited with a 24 eV primary electron.¹⁵ In the situation where K_+ is set to be zero and both emitted electrons have the same kinetic energy the most likely angle between the trajectories is 50° . This would mean for our kinetic energy electrons a value of $K_\pm \pm 0.44$ a.u., which is smaller than the value we have observed in Fig. 7(d). This observation is at odds with the interpretation of the outer peaks in the distribution of Fig. 7(d) to come from a single photo electron, which collides with a valence band electron. However, we can not directly transfer the results of this $(e, 2e)$ calculation on our data from $(\gamma, 2e)$ as in the latter case one has to sum over a more complex initial state for the projectile electron. Undoubtedly, we observe a dependency on the light polarization, but a simple explanation by means of the propensity rule is not sufficient. This means that this rule is not strictly true but is only approximately true.

IV. SUMMARY

We have applied a new time-of-flight projection technique to image the double electron emission process from surfaces after single photon absorption. The high angular acceptance allows for a comprehensive view on the emission dynamics. In the coincident angular distributions, we find a strong dependency of the individual electrons on the energy sharing and relative angles. For equal energy sharing, a pronounced

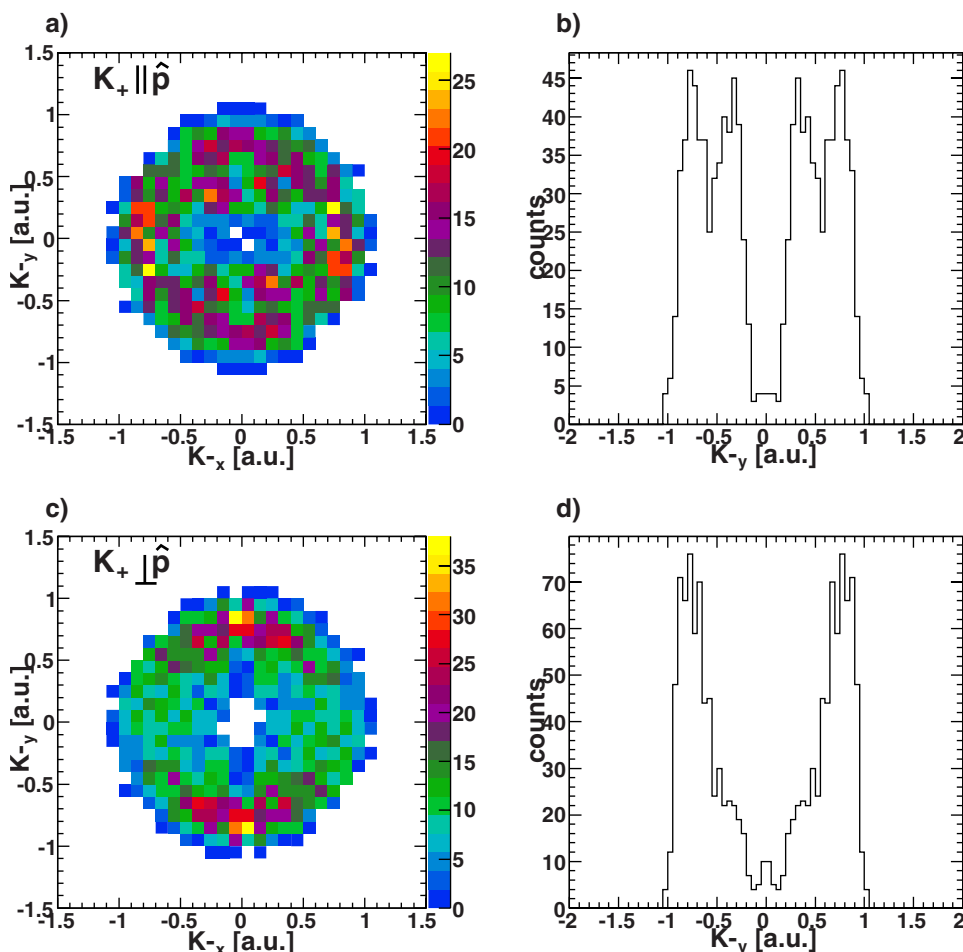


FIG. 7. (Color online) Distribution of relative momenta for different orientations of the sum momentum in respect to the polarization vector. $\hbar\omega$ is 40 eV and sum energies $E_1 + E_2 = \hbar\omega - 2W_\phi \pm 3$ eV, equal energy sharing. (a) Sum momentum parallel to polarization and (c) sum momentum perpendicular to polarization. (b) and (d) are projections of the area $K_{-x} \pm 0.3$ a.u. to the Y axis.

decrease in the signal is observed if the intermediate angle between the two electrons is small, which can be regarded as signature of the exchange-correlation hole. Evaluating the data in a center-of-mass frame yields a value for the smallest distance of the two electrons in momentum space of 0.76 a.u. Focusing on events for which K_+ is either perpendicular or parallel to the polarization vector reveals that the propensity rule for DPE is not strictly valid. We do observe a strong dependence of the behavior of K_+ with respect to the light polarization, which was previously

not observed. The cause of this behavior needs to be clarified.

ACKNOWLEDGMENTS

We would like to thank R. Döhrmann, T. Möller, and the HASYLAB staff for their support and Roentdek GmbH for providing the multihit detection equipment. This work was supported in part by the Bundesministerium für Bildung und Forschung (BMBF).

*hattass@atom.uni-frankfurt.de

- ¹Yu. F. Smirnov, A. V. Pavlitchenkov, V. G. Levin, and V. G. Neudatschin, *J. Phys. B* **11**, 3587 (1978).
- ²V. G. Levin, V. G. Neudatchin, A. V. Pavlitchankov, and Yu. F. Smirnov, *J. Phys. B* **17**, 1525 (1984).
- ³T. Weber, A. O. Czasch, O. Jagutzki, A. K. Müller, V. Mergel, A. Kheifets, E. Rotenberg, G. Meigs, M. H. Prior, S. Daveau, A. Landers, C. L. Cocke, T. Osipov, R. Diez Muino, H. Schmidt-Böcking, and R. Dörner, *Nature (London)* **431**, 437 (2004).
- ⁴W. Vanroose, F. Martin, T. N. Rescigno, and C. W. McCurdy, *Science* **310**, 1787 (2005).
- ⁵L. Spielberger, O. Jagutzki, R. Dörner, J. Ullrich, U. Meyer, V.

- Mergel, M. Unverzagt, M. Damrau, T. Vogt, I. Ali, Kh. Khayyat, D. Bahr, H. G. Schmidt, R. Frahm, and H. Schmidt-Böcking, *Phys. Rev. Lett.* **74**, 4615 (1995).
- ⁶L. Spielberger, O. Jagutzki, B. Krässig, U. Meyer, Kh. Khayyat, V. Mergel, Th. Tschentscher, Th. Buslaps, H. Bräuning, R. Dörner, T. Vogt, M. Achler, J. Ullrich, D. S. Gemmell, and H. Schmidt-Böcking, *Phys. Rev. Lett.* **76**, 4685 (1996).
- ⁷K. A. Kouzakov and J. Berakdar, *Phys. Rev. Lett.* **91**, 257007 (2003).
- ⁸O. Schwarzkopf, B. Krässig, J. Elmiger, and V. Schmidt, *Phys. Rev. Lett.* **70**, 3008 (1993).
- ⁹J. McGuire, N. Berrah, R. Bartlett, J. Samson, J. Tanis, C.

- Cocke, and A. Schlachter, *J. Phys. B* **28**, 913 (1995).
- ¹⁰J. Briggs and V. Schmidt, *J. Phys. B* **33**, R1 (2000).
- ¹¹R. Dörner, H. Schmidt-Böcking, Th. Weber, T. Jahnke, M. Schöffler, A. Knapp, M. Hattass, A. Czasch, L. Ph. Schmidt, and O. Jagutzki, *Radiat. Phys. Chem.* **70**, 191 (2004).
- ¹²W. Kohn and L. J. Sham, *Phys. Rev.* **140**, A1133 (1965).
- ¹³W. Kohn, *Rev. Mod. Phys.* **71**, 1253 (1999).
- ¹⁴N. Fominykh, J. Berakdar, J. Henk, and P. Bruno, *Phys. Rev. Lett.* **89**, 086402 (2002).
- ¹⁵H. Gollisch, N. v. Schwartzberg, and R. Feder, *Phys. Rev. B* **74**, 075407 (2006).
- ¹⁶J. C. Slater, *Rev. Mod. Phys.* **6**, 209 (1934).
- ¹⁷H. W. Biester, M. J. Besnard, G. Dujardin, L. Hellner, and E. E. Koch, *Phys. Rev. Lett.* **59**, 1277 (1987).
- ¹⁸R. Herrmann, S. Samarin, H. Schwabe, and J. Kirschner, *Phys. Rev. Lett.* **81**, 2148 (1998).
- ¹⁹F. O. Schumann, C. Winkler, G. Kerherve, and J. Kirschner, *Phys. Rev. B* **73**, 041404(R) (2006).
- ²⁰F. O. Schumann, C. Winkler, and J. Kirschner, *Phys. Rev. Lett.* **98**, 257604 (2007).
- ²¹O. Jagutzki, A. Cerezo, A. Czasch, R. Dörner, M. Hattass, M. Huang, V. Mergel, U. Spillmann, K. Ullmann-Pfeifer, T. Weber, H. Schmidt-Böcking, and G. D. W. Smith, *IEEE Trans. Nucl. Sci.* **49**, 2477 (2002).
- ²²Roentdek GmbH, see www.roentdek.de for details
- ²³M. Hattass, T. Jalowy, A. Czasch, Th. Weber, T. Jahnke, S. Schössler, L. Ph. Schmidt, O. Jagutzki, R. Dörner, and H. Schmidt-Böcking, *Rev. Sci. Instrum.* **75**, 2373 (2004).
- ²⁴S. Hüfner, *Photoelectron Spectroscopy* (Springer, Berlin, 1995), and references therein.
- ²⁵J. Berakdar, *Phys. Rev. B* **58**, 9808 (1998).
- ²⁶R. Dörner, J. M. Feagin, C. L. Cocke, H. Bräuning, O. Jagutzki, M. Jung, E. P. Kanter, H. Khemliche, S. Kravis, V. Mergel, M. H. Prior, H. Schmidt-Böcking, L. Spielberger, J. Ullrich, M. Unverzagt, and T. Vogt, *Phys. Rev. Lett.* **77**, 1024 (1996).
- ²⁷A. Knapp, M. Walter, Th. Weber, A. L. Landers, S. Schössler, T. Jahnke, M. Schöffler, J. Nickles, S. Kammer, O. Jagutzki, L. Ph. H. Schmidt, T. Osipov, J. Rösch, M. H. Prior, H. Schmidt-Böcking, C. L. Cocke, J. Feagin, and R. Dörner, *J. Phys. B* **35**, L521 (2002).